

Breaking the centrifugal barrier to giant planet contraction by magnetic disc braking

Sivan Ginzburg¹*† and Eugene Chiang^{1,2}

¹*Department of Astronomy, University of California at Berkeley, CA 94720-3411, USA*

²*Department of Earth and Planetary Science, University of California at Berkeley, CA 94720-4767, USA*

Accepted XXX. Received YYY; in original form ZZZ

ABSTRACT

During the runaway phase of their formation, gas giants fill their gravitational spheres of influence out to Bondi or Hill radii. When runaway ends, planets shrink several orders of magnitude in radius until they are comparable in size to present-day Jupiter; in 1D models, the contraction occurs on the Kelvin–Helmholtz time-scale t_{KH} , which is initially a few thousand years. However, if angular momentum is conserved, contraction cannot complete, as planets are inevitably spun up to their breakup periods P_{break} . We consider how a circumplanetary disc (CPD) can de-spin a primordially magnetized gas giant and remove the centrifugal barrier, provided the disc is hot enough to couple to the magnetic field, a condition that is easier to satisfy at later times. By inferring the planet’s magnetic field from its convective cooling luminosity, we show that magnetic spin-down times are shorter than contraction times throughout post-runaway contraction: $t_{\text{mag}}/t_{\text{KH}} \sim (P_{\text{break}}/t_{\text{KH}})^{1/21} \lesssim 1$. Planets can spin down until they corotate with the CPD’s magnetospheric truncation radius, at a period $P_{\text{max}}/P_{\text{break}} \sim (t_{\text{KH}}/P_{\text{break}})^{1/7}$. By the time the disc disperses, $P_{\text{max}}/P_{\text{break}} \sim 20\text{--}30$; further contraction at fixed angular momentum can spin planets back up to $\sim 10P_{\text{break}}$, potentially explaining observed rotation periods of giant planets and brown dwarfs.

Key words: planets and satellites: formation – planets and satellites: gaseous planets – planets and satellites: magnetic fields – planet–disc interactions

1 INTRODUCTION

Gas giants are thought to form when gas from an ambient circumstellar disc cools atop a rocky or icy core (e.g. Bodenheimer & Pollack 1986; Pollack et al. 1996; Ikoma et al. 2000). The planet’s proto-atmosphere extends to the smaller of the Bondi radius and the Hill radius, both of which are several orders of magnitude larger than present-day Jupiter. Atmospheric gas cools and contracts on a Kelvin–Helmholtz (KH) time-scale, allowing fresh nebular gas to flow in and take its place. Once the atmosphere outweighs the core, the KH time-scale begins to decrease with increasing mass, and the planet cools and grows at an ever faster, ‘runaway’ rate.

Accretion is also limited by the nebula’s ability to supply gas at a sufficient rate to the Bondi/Hill radius to keep up with the planet’s increasingly shorter cooling and contraction time. The rate of supply is capped by the radial transport rate through the disc, and further limited by the opening of annular gaps (depleted cav-

ities) around the planet’s orbit. Both of these effects can put an end to runaway growth (Lin & Papaloizou 1993; Kley 1999; Tanigawa & Ikoma 2007; Lissauer et al. 2009; Tanigawa & Tanaka 2016; Ginzburg & Chiang 2019b; Lee 2019). Post-runaway planetary accretion is not zero; it persists up to the eventual dispersal of the disc in a few million years’ time (Mamajek 2009; Pfalzner et al. 2014), and can be responsible for doubling the planet’s mass or more (Mordasini et al. 2012; Ginzburg & Chiang 2019a).

In the post-runaway phase, because of insufficient gas supply, the planet no longer fills the Bondi/Hill radius but detaches from the nebula to contract on the KH time-scale (Bodenheimer et al. 2000; Mordasini et al. 2012, 2017; Ginzburg & Chiang 2019a). Previous one-dimensional models assumed the planet is free to shrink by orders of magnitude until its radius is comparable to that of Jupiter. However, planets spin up as they contract as a consequence of angular momentum conservation. Eventually they hit up against a centrifugal barrier: when the planet spins at breakup velocity, it cannot contract further without shedding spin angular momentum. To aggravate the problem, the spin of the planet at the end of runaway growth will

* E-mail: ginzburg@berkeley.edu

† 51 Pegasi b Fellow.

already be close to breakup if it accretes mass with the Keplerian shear velocity across the Hill sphere.

Possible mechanisms to dispose of excess angular momentum include expulsion of material, once breakup is reached, into a circumplanetary disc (CPD; Ward & Canup 2010) and magnetic interaction between the planet and such a disc (Takata & Stevenson 1996). Batygin (2018) demonstrated that magnetic planet–CPD interaction can explain the observed sub-breakup spins of young extra-solar gas giants (Bryan et al. 2018). The same spin regulation mechanism can be invoked for isolated brown dwarfs and T-Tauri stars (objects without a stellar companion); in these cases the CPD and primary disc are one and the same (see Koenigl 1991; Armitage & Clarke 1996).¹ While Batygin (2018) focused on the terminal rotation of planets and evolved them from an initial condition of twice the radius of Jupiter, here we expand the scope of the theory to cover earlier times, and ask whether planets can contract starting from as large a radius as the Bondi/Hill radius. We utilize the Christensen et al. (2009) scaling to relate a planet’s magnetic field to its convective luminosity and thence to its KH contraction time, thereby self-consistently evolving the planet’s radius and magnetic field over the entire duration of post-runaway accretion.

The rest of this letter is organized as follows. We describe the planetary magnetic field and its coupling to the CPD in Section 2, and calculate the planet’s spin evolution in Section 3. We compare our theory with observations of rotation periods in Section 4, and summarize in Section 5.

2 MAGNETIC COUPLING

We present a model for the magnetic interaction between a nascent planet and its CPD. The treatment is similar to that of Batygin (2018). We omit order-unity coefficients to focus on scaling relations.

2.1 Magnetic field

Christensen et al. (2009) proposed that the magnetic field strength B of a planet of mass M and radius R is determined by equipartition of energy, with the magnetic energy density comparable to the kinetic energy density of the convective flow that transports the planet’s internal luminosity L :

$$B^2 \sim \rho v_{\text{conv}}^2 \sim \rho^{1/3} \left(\frac{L}{R^2} \right)^{2/3}, \quad (1)$$

where $\rho \sim M/R^3$ is the planet’s mean density, v_{conv} is the convective velocity, and $L/R^2 \sim \rho v_{\text{conv}}^3$ is the convective flux. Christensen et al. (2009) demonstrated that this scaling fits both solar system planets and rapidly rotating stars. Recent observations seem to also validate this scaling for hot Jupiters; these emit a higher internal luminosity compared

to Jupiter, and are therefore expected to maintain a stronger field (Yadav & Thorngrén 2017; Cauley et al. 2019).

Throughout most of the evolution discussed here, planets remain larger than $2R_J$, where R_J is the radius of Jupiter (Ginzburg & Chiang 2019a). Under such conditions, electron degeneracy and electrostatic interactions are negligible, and the planets can be modelled with an ideal gas equation of state. The effects of degeneracy, which might play a role during the latest stages of contraction, are discussed in the appendix. For non-degenerate objects, the KH time-scale is given by

$$t_{\text{KH}} \sim \frac{GM^2}{RL}, \quad (2)$$

where G is the gravitational constant. We rewrite equation (1) as

$$B \sim \left(\frac{GM^2}{R^4} \right)^{1/2} \left(\frac{P_{\text{break}}}{t_{\text{KH}}} \right)^{1/3}, \quad (3)$$

with $P_{\text{break}} \sim (GM/R^3)^{-1/2}$ denoting the planet’s breakup rotation period.

2.2 Truncation radius

If the magnetic field is strong enough, the CPD does not extend all the way to the planet’s surface. Close enough to the planet, the magnetic energy density exceeds the kinetic energy density of the accretion flow, truncating the disc at an inner radius

$$R_t \sim \left(\frac{\mu^4}{GM\dot{M}^2} \right)^{1/7}, \quad (4)$$

where $\mu = BR^3$ is the planet’s magnetic dipole moment and \dot{M} is the mass accretion rate (Elsner & Lamb 1977; Ghosh & Lamb 1979; Koenigl 1991; Ostriker & Shu 1995; Mohanty & Shu 2008). Equation (4) is appropriate for spherically symmetric accretion, or for accretion through an equatorial disc in which the flow transitions from Keplerian to magnetospheric over a radial length scale comparable to the disc radius (e.g. Shapiro & Teukolsky 1983, section 15.2). The geometry of our problem is different; three-dimensional simulations of planets embedded in circumstellar discs find that a planet accretes mainly through its poles, and forms a decretion disc at the equator (Tanigawa et al. 2012; Morbidelli et al. 2014; Fung et al. 2015; Fung & Chiang 2016; Szulágyi et al. 2016). We ignore these complications and assume that equation (4) gives the truncation radius of the equatorial decretion disc. The same assumption was made by Batygin (2018). If nothing else, the dipole geometry of the magnetic field, whose energy density dominates at $r < R_t$, should help to enforce a roughly spherical magnetosphere.

In Ginzburg & Chiang (2019a) we explained that during post-runaway accretion the planet adjusts its contraction to satisfy $t_{\text{KH}} = M/\dot{M}$. This condition was derived neglecting spin angular momentum; however, we will find below that magnetic spin-down is efficient and that contraction can proceed on the KH time-scale, with the planet radiating away the accretion luminosity $L = GM\dot{M}/R$. Using this relation, and substituting B from equation (3), we rewrite equation

¹ Magnetic braking also occurs when spin angular momentum is carried away by a magnetized wind emanating from the object. Wind braking seems too weak to explain the slow rotation of low-mass stars and brown dwarfs that are a few Myr old (Kawaler 1988; Bouvier et al. 2014; Moore et al. 2019).

(4) as

$$\frac{R_t}{R} \sim \left(\frac{t_{\text{KH}}}{P_{\text{break}}} \right)^{2/21} > 1. \quad (5)$$

The magnetic field always truncates the disc ($R_t > R$) in our case because the thermal time-scale t_{KH} is orders of magnitude longer than P_{break} (see Section 3).

2.3 Magnetic torque

Magnetic field lines that originate from the planet rotate at its spin frequency ω and puncture the CPD. At any given radius r in the disc, if the Keplerian orbital angular velocity $(GM/r^3)^{1/2}$ differs from ω , the field lines are twisted by the disc, generating a counter-torque. The total torque that the disc exerts on the planet is given by

$$T \sim \int_{R_t} \frac{\mu^2}{r^4} dr \sim B^2 R^3 \left(\frac{R}{R_t} \right)^3 \quad (6)$$

(for details, see Livio & Pringle 1992; Armitage & Clarke 1996; Spalding & Batygin 2015; Batygin 2018). The magnitude and sign of the torque are dictated by the inner edge of the disc at R_t . If the inner edge rotates slower (faster) than the planet, the torque will spin the planet down (up). Following Batygin (2018), we assume that the CPD is connected to the larger circumstellar disc such that whatever angular momentum (of whatever sign) is transferred from the planet to the CPD is subsequently transferred to the nebula at large. In equilibrium, the planet nearly corotates with the disc's edge: $\omega^2 \sim GM/R_t^3$.

2.4 Electrical conductivity

We have assumed in the above that the disc is sufficiently electrically conductive that it couples to the planetary magnetosphere. A measure of the coupling is the magnetic Reynolds number \mathcal{R}_m which needs to be $\gg 1$ (otherwise, field lines diffuse rather than advect and twist under the Keplerian disc flow). Batygin (2018) evaluated \mathcal{R}_m using the Keplerian velocity and the disc scale height (their equation 4).² We will adopt this same definition, and use their result that $\mathcal{R}_m > 1$ when the temperature $T > 750$ K, which follows from thermal ionization of trace alkali metals (their fig. 1). This prescription overestimates the electrical conductivity insofar as charge-adsorbing dust grains are ignored, but also underestimates the conductivity because it neglects non-thermal sources of ionization, e.g. ultraviolet radiation. For simplicity we take T to be that of the planet's photosphere. Our value of T may be an underestimate because it ignores other sources of heating such as shocks or dissipative

² This choice yields a value intermediate between other choices for \mathcal{R}_m : a smaller one which replaces the Keplerian velocity with the disc sound speed (this \mathcal{R}_m is typically used to gauge whether the disc can sustain magneto-rotational turbulence; e.g. Fleming et al. 2000), and a larger one which replaces the disc scale height with the disc radius (this \mathcal{R}_m was used by Turner & Sano 2008 to gauge whether toroidal fields could be generated by disc Keplerian shear from radial fields).

magnetospheric processes; these appear implicated by detections of H α emission from planet candidates (Wagner et al. 2018; Haffert et al. 2019; Thanathibodee et al. 2019).

In Fig. 1 we mark, for each of the evolutionary tracks described in Section 3, the time when the accreting planet's photosphere exceeds 750 K. The model for $\kappa = 10^{-1} \text{ cm}^2 \text{ g}^{-1}$ and $\beta = 15$ does not exceed this threshold temperature and so may not be magnetically coupled, modulo the many uncertainties regarding heating and ionization listed above. The other models (including all the models that reach a high mass) are nominally coupled starting at times $t \gtrsim 0.1$ –1 Myr, depending on β (the accretion history) and κ (the opacity). This helps to justify our analysis of the observations in Section 4, which are of suitably old and massive systems.

3 SPIN EVOLUTION

If spin angular momentum were strictly conserved, a contracting planet would eventually reach breakup rotation and cease contracting (Section 1). However, the disc can remove spin angular momentum by magnetic torques. Shedding as much as the breakup angular momentum takes a time

$$t_{\text{mag}} \sim \frac{MR^2 \sqrt{GM/R^3}}{T}. \quad (7)$$

Using equations (3), (5), and (6):

$$\frac{t_{\text{mag}}}{t_{\text{KH}}} \sim \left(\frac{P_{\text{break}}}{t_{\text{KH}}} \right)^{1/21} \lesssim 1. \quad (8)$$

Since P_{break} is many orders of magnitude smaller than t_{KH} , equation (8) implies at face value that $t_{\text{mag}} < t_{\text{KH}}$, but only by a factor of a few because $P_{\text{break}}/t_{\text{KH}}$ is taken to a weak power. This result is relatively insensitive to the magnetic field B because of two competing effects that nearly cancel out: a stronger field amplifies the torque exerted at a given radius r , but it also truncates the disc at a larger $R_t \propto B^{4/7}$. The total torque scales as $T \propto B^2/R_t^3 \propto B^{2/7}$.

Equation (8) indicates that, modulo an uncertain order-unity coefficient, magnetic coupling to CPDs may spin planets down somewhat faster than contraction spins them up. We conclude that angular momentum does not present a significant barrier to contraction, which can proceed on approximately the KH time-scale while the planet is regulated to spin slower than breakup. This helps to justify previous one-dimensional calculations that did not consider spin.

In Fig. 1 we plot four example evolutionary tracks for spin and magnetic field. The tracks represent different post-runaway cooling and accretion models, as computed in figs 1–4 of Ginzburg & Chiang (2019a). In that paper, we parametrized the post-runaway accretion rate \dot{M} with a power law $M/\dot{M} \propto M^\beta$, and numerically solved the planet's concurrent accretion and contraction history. We accounted for zones of hydrogen dissociation and ionization in the planet's interior, and also considered two values for the opacity at the radiative-convective boundary, $\kappa = 10^{-1}$ and $10^{-2} \text{ cm}^2 \text{ g}^{-1}$, to account for gas with and without dust, respectively. In the $\beta = 15$ models, which are inspired by planets opening gaps in practically inviscid discs, gas accretion drops more drastically after the end of runaway growth, producing planets with a final mass slightly less than Jupiter ($0.8 M_J$).

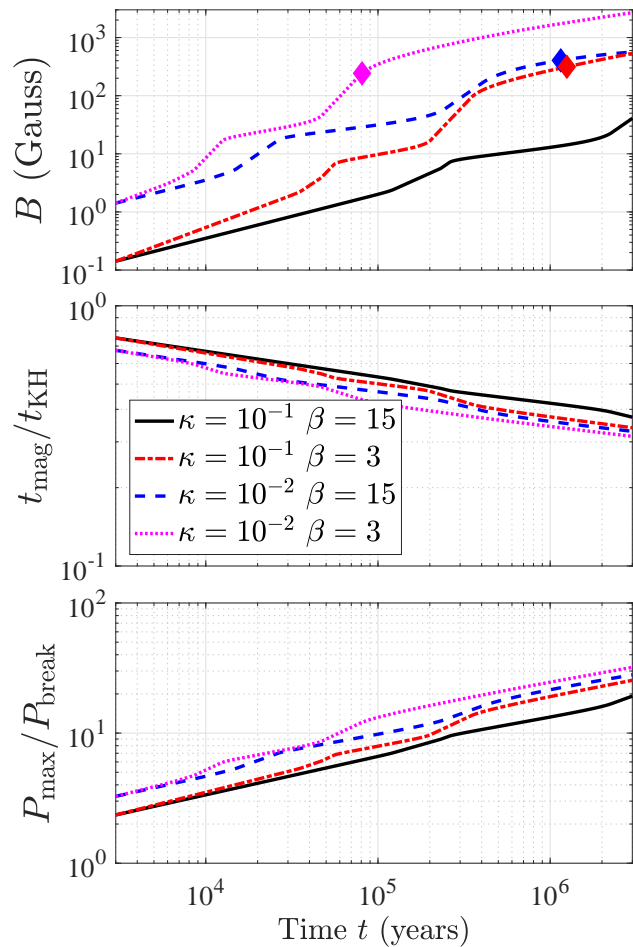


Figure 1. Evolution of planetary spin and magnetic field post-runaway, for the four models in Ginzburg & Chiang (2019a). Time is measured since the end of runaway growth, after which the planet mass doubles on a time-scale that grows with mass as $M/\dot{M} \propto M^\beta$. The opacity κ at the planet’s radiative–convective boundary is given in units of $\text{cm}^2 \text{g}^{-1}$. The magnetic field B (top panel) is given by equation (3). The magnetic spin-down time t_{mag} (middle panel) is given by equation (8) and is nominally shorter than the Kelvin–Helmholtz contraction time t_{KH} by factors of a few. The inequality $t_{\text{mag}} \lesssim t_{\text{KH}}$ implies that the rotation period is regulated to be less than the breakup period P_{break} and that the planet contracts on the thermal time without much interference from centrifugal forces. The planet can spin down until it corotates with the magnetic truncation radius of the circumplanetary disc, at a period P_{max} (bottom panel), given by equation (9). Diamonds mark when the accreting planet’s photosphere becomes hot enough to thermally ionize the disc’s inner edge to magnetic Reynolds numbers $\mathcal{R}_m > 1$ and thereby couple it to the planet’s magnetic field. This threshold condition is conservative insofar as other heating and ionization mechanisms are neglected (see Section 2.4). The solid black curve never crosses this threshold.

By comparison, in the $\beta = 3$ models, which derive from planets opening gaps in more viscous discs, masses grow to about $5 M_J$. In low-opacity models, planets cool and contract to a radius of approximately $2 R_J$ by the time the disc expires at $t_{\text{disc}} = 3$ Myr. In the high-opacity models, the planets remain inflated at about $7 R_J$ at that time.

While the four combinations of β and κ span a range

of possible evolutions, Fig. 1 demonstrates that our conclusions for spin appear robust. Despite a wide range of possible magnetic field strengths, the magnetic spin-down time t_{mag} is nominally always shorter than the KH cooling time t_{KH} . As the planet contracts, its breakup period P_{break} decreases, whereas t_{KH} increases. Thus $P_{\text{break}}/t_{\text{KH}}$ decreases with time, and by extension so does $t_{\text{mag}}/t_{\text{KH}}$ by equation (8).

How much slower does the planet spin relative to breakup? As discussed in Section 2.3, planets seek an equilibrium where they corotate with the disc’s magnetic truncation radius R_t . Using equation (5), corotation sets a limiting rotation period given by

$$\frac{P_{\text{max}}}{P_{\text{break}}} \sim \left(\frac{R_t}{R}\right)^{3/2} \sim \left(\frac{t_{\text{KH}}}{P_{\text{break}}}\right)^{1/7} \quad (9)$$

as plotted in the bottom panel of Fig. 1. The time-scale to establish corotation is comparable to t_{mag} if the planet starts at breakup, and shorter than t_{mag} if it starts slower than breakup. We argued from equation (8) that $t_{\text{mag}}/t_{\text{KH}} < 1$, which would imply that planets maintain corotation as they contract. However, the margin by which t_{mag} is less than t_{KH} is small and uncertain (owing to the weak exponent in equation 8 and the unknown coefficient), and so we allow for the possibility that corotation equilibrium might not quite be reached. Thus it is safer to regard P_{max} as an upper limit on the true spin period (and P_{break} as a lower limit). By the end of the disc’s lifetime, when $t_{\text{KH}} = t_{\text{disc}} = 3$ Myr (e.g. Ginzburg & Chiang 2019a), planets rotate up to 20–30 times slower than breakup.

4 OBSERVATIONS

Bryan et al. (2018) measured the rotation periods of several directly-imaged planets and low-mass brown dwarfs, compiling a sample that included theirs and previous observations. These objects have ages of 2–300 Myr, and their parent discs have all completely dissipated. We plot the rotation periods and masses of the Bryan et al. (2018) sample in Fig. 2, overlaying our theoretical estimates of the maximal rotation period P_{max} relative to the breakup period P_{break} . Note that $P_{\text{break}} \propto R^{3/2}$, and the radius R at the time of disc dispersal depends on atmospheric opacity; the theoretical curves in Fig. 2 employ two possible radii, $2 R_J$ for dust-free atmospheres, and $7 R_J$ for dusty ones (Ginzburg & Chiang 2019a).

Fig. 2 demonstrates that real-life gas giants and brown dwarfs respect the upper bound on spin periods set by magnetic coupling to CPDs. If we imagine that planets start at $P/P_{\text{break}} \sim P_{\text{max}}/P_{\text{break}} \approx 20\text{--}30$ at the time of disc dispersal, and subsequently preserve their spin angular momentum while contracting and spinning up as $P/P_{\text{break}} \propto R^{1/2}$, then the final observed P/P_{break} will drop from its initial value by a factor of a few. This scenario may explain why many of the data points appear to cluster around $P/P_{\text{break}} \approx 10$.

Whether there is a trend in P/P_{break} with M is unclear. Bryan et al. (2018) did not find any of statistical significance. Fig. 2 gives the same impression, especially if we omit the one point with the lowest mass—and note that there is an observational bias against detecting slowly rotating, low-mass objects, as these will be among the faintest, with atmospheric lines hardest to spectrally resolve. The absence of a correlation appears consistent with theory; the $1/7$ power

in equation (9) flattens all trends. More data are needed at low M to see whether this agreement continues to hold.

5 SUMMARY

During the initial cooling-limited phase of its growth, a nascent gas giant fills its gravitational sphere of influence (out to the Bondi or Hill radius) as it accumulates mass at its periphery faster than it can contract. Accretion in this phase eventually runs away with the increasing self-gravity of the gaseous envelope. When runaway growth ends—because of gaps opened by the planet in its parent disc, and limitations in the rate at which the disc can transport mass—the planet’s radius is finally free to begin contracting on the Kelvin–Helmholtz cooling time-scale t_{KH} , which is initially as short as a few 10^3 years. During this post-runaway phase, accretion continues even as the planet shrinks (Mordasini et al. 2012; Ginzburg & Chiang 2019a). The radius must decrease by several orders of magnitude before it attains the present-day observed value for Jupiter. The problem is that without a mechanism to remove the planet’s spin angular momentum, contraction stalls as the planet is inevitably spun up to breakup speed.

In this letter we considered magnetic coupling of the planet to a circumplanetary disc (CPD) as a means to shed angular momentum and spin the planet down (Takata & Stevenson 1996; Batygin 2018). New theoretical arguments and observations link the planet’s magnetic field to its luminosity (Christensen et al. 2009; Yadav & Thorngrén 2017; Cauley et al. 2019) and thereby to t_{KH} . These connections enabled us to consistently compare the magnetic spin-down time t_{mag} to t_{KH} throughout the planet’s contraction history, and to extend the calculation of Batygin (2018) to earlier times, when the planet is much larger than present-day Jupiter. The theory applies also for objects without a stellar host (e.g. isolated brown dwarfs); the only requirement is that the object be surrounded by a disc that can shuttle angular momentum away to large distance.

We found that at any given time during contraction, $t_{\text{mag}}/t_{\text{KH}} \sim (P_{\text{break}}/t_{\text{KH}})^{1/21}$, where P_{break} is the breakup rotation period. Since $P_{\text{break}}/t_{\text{KH}} \ll 1$, $t_{\text{mag}}/t_{\text{KH}} \lesssim 1$, indicating that planets are marginally able to shed their angular momentum while contracting on the Kelvin–Helmholtz time-scale. That is, the angular momentum barrier to planetary contraction can be largely removed by CPDs interacting with primordially strong planetary magnetic fields. An underlying assumption is that the CPD is sufficiently ionized to couple to the planet’s magnetosphere; this assumption might fail at early times, especially for low-mass planets.

In addition to justifying the results of previous studies of giant planet formation that did not explicitly consider spin, we also calculated how the rotation periods of gas giants evolve during post-runaway accretion. We found that planets rotate slower than breakup, with a maximal rotation period given by $P_{\text{max}}/P_{\text{break}} \sim (t_{\text{KH}}/P_{\text{break}})^{1/7}$. This ratio gradually increases with time as long as the CPD can transfer angular momentum from the planet to the nebula at large. When the parent disc finally expires at a time $t_{\text{disc}} \sim t_{\text{KH}} \sim 3$ Myr, $P_{\text{max}}/P_{\text{break}} \approx 20\text{--}30$ in a variety of post-runaway models (Fig. 1). Contraction at fixed angular momentum after the

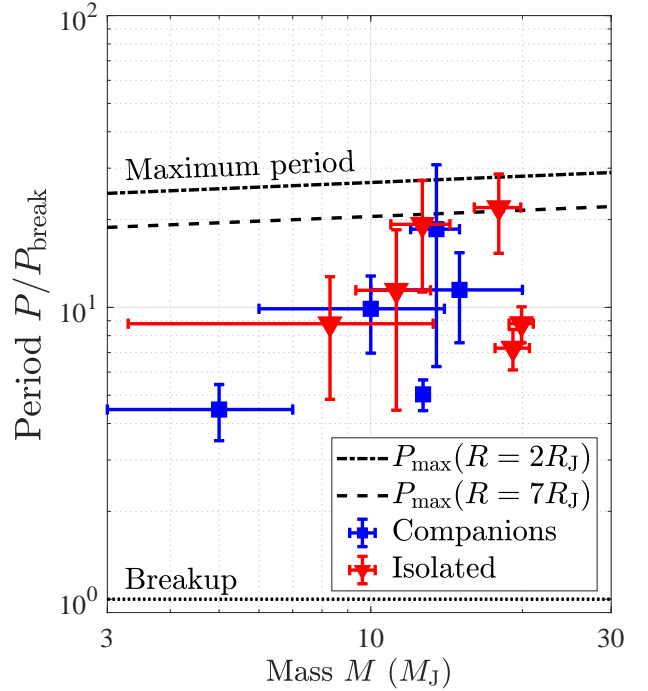


Figure 2. Rotation periods relative to breakup of young sub-stellar companions (blue squares) and isolated brown dwarfs (red triangles), taken from Bryan et al. (2018) with updated error bars (M. Bryan 2019, personal communication). The sloped dashed black lines show the longest rotation periods P_{max} , normalized to breakup periods P_{break} , to which objects may be spun down by magnetic coupling to circumplanetary (or circum-brown dwarf) discs. The ratio $P_{\text{max}}/P_{\text{break}}$, given by equation (9) with t_{KH} equated to the disc lifetime $t_{\text{disc}} = 3$ Myr, is evaluated for two values of the object’s radius $R = 2R_{\text{J}}, 7R_{\text{J}}$; these give different breakup periods at the time of disc dispersal ($P_{\text{break}} \propto R^{3/2}$), with the smaller radius corresponding to contraction of a relatively low-opacity dust-free atmosphere. After the disc dissipates, continued contraction at fixed angular momentum lowers $P/P_{\text{break}} \propto R^{1/2}$ by a factor of a few below the sloped black lines, possibly explaining why the observations cluster there.

disc vanishes may spin planets back up to $P_{\text{max}}/P_{\text{break}} \sim 10$, potentially explaining observed rotation periods of young planets and low-mass brown dwarfs (Fig. 2).

While we have focused on the magnitude of planetary spin, future work can examine the direction of the spin vector, i.e. the relative orientations of CPDs and planetary magnetic/spin axes (Lai et al. 2011; Spalding & Batygin 2015). The CPD might not necessarily be aligned with the parent circumstellar disc, particularly in turbulent discs. Obliquities of sub-stellar objects are beginning to be measured (Bryan et al. 2019).

ACKNOWLEDGEMENTS

We thank Marta Bryan for discussions and for providing the Bryan et al. (2018) data. We thank Konstantin Batygin and the anonymous reviewer for comments which improved the letter. SG is supported by the Heising-Simons Foundation through a 51 Pegasi b Fellowship. This work benefited from NASA’s Nexus for Exoplanet System Science (NExSS) re-

search coordination network sponsored by NASA's Science Mission Directorate (NNX15AD95G/NEXSS).

REFERENCES

- Armitage P. J., Clarke C. J., 1996, *MNRAS*, **280**, 458
 Batygin K., 2018, *AJ*, **155**, 178
 Bodenheimer P., Pollack J. B., 1986, *Icarus*, **67**, 391
 Bodenheimer P., Hubickyj O., Lissauer J. J., 2000, *Icarus*, **143**, 2
 Bouvier J., Matt S. P., Mohanty S., Scholz A., Stassun K. G., Zanni C., 2014, in Beuther H., Klessen R. S., Dullemond C. P., Henning T., eds, *Protostars and Planets VI*. p. 433, doi:10.2458/azu_uapress_9780816531240-ch019
 Bryan M. L., Benneke B., Knutson H. A., Batygin K., Bowler B. P., 2018, *Nature Astronomy*, **2**, 138
 Bryan M. L., Bowler B., Blunt S., Ngo H., Morley C., Mawet D., 2019, in *AAS/Division for Extreme Solar Systems Abstracts*. p. 202.06
 Cauley P. W., Shkolnik E. L., Llama J., Lanza A. F., 2019, *Nature Astronomy*, p. 408
 Christensen U. R., Holzwarth V., Reiners A., 2009, *Nature*, **457**, 167
 Elsner R. F., Lamb F. K., 1977, *ApJ*, **215**, 897
 Fleming T. P., Stone J. M., Hawley J. F., 2000, *ApJ*, **530**, 464
 Fung J., Chiang E., 2016, *ApJ*, **832**, 105
 Fung J., Artymowicz P., Wu Y., 2015, *ApJ*, **811**, 101
 Ghosh P., Lamb F. K., 1979, *ApJ*, **232**, 259
 Ginzburg S., Chiang E., 2019a, doi:10.1093/mnras/stz2901
 Ginzburg S., Chiang E., 2019b, *MNRAS*, **487**, 681
 Haffert S. Y., Bohn A. J., de Boer J., Snellen I. A. G., Brinchmann J., Girard J. H., Keller C. U., Bacon R., 2019, *Nature Astronomy*, p. 329
 Ikoma M., Nakazawa K., Emori H., 2000, *ApJ*, **537**, 1013
 Kawaler S. D., 1988, *ApJ*, **333**, 236
 Kley W., 1999, *MNRAS*, **303**, 696
 Koenigl A., 1991, *ApJ*, **370**, L39
 Lai D., Foucart F., Lin D. N. C., 2011, *MNRAS*, **412**, 2790
 Lee E. J., 2019, *ApJ*, **878**, 36
 Lin D. N. C., Papaloizou J. C. B., 1993, in Levy E. H., Lunine J. I., eds, *Protostars and Planets III*. p. 749
 Lissauer J. J., Hubickyj O., D'Angelo G., Bodenheimer P., 2009, *Icarus*, **199**, 338
 Livio M., Pringle J. E., 1992, *MNRAS*, **259**, 23P
 Mamajek E. E., 2009, in Usuda T., Tamura M., Ishii M., eds, Vol. 1158, *American Institute of Physics Conference Series*. pp 3–10 (arXiv:0906.5011), doi:10.1063/1.3215910
 Mohanty S., Shu F. H., 2008, *ApJ*, **687**, 1323
 Moore K., Scholz A., Jayawardhana R., 2019, *ApJ*, **872**, 159
 Morbidelli A., Szulágyi J., Crida A., Lega E., Bitsch B., Tanigawa T., Kanagawa K., 2014, *Icarus*, **232**, 266
 Mordasini C., Alibert Y., Klahr H., Henning T., 2012, *A&A*, **547**, A111
 Mordasini C., Marleau G. D., Mollière P., 2017, *A&A*, **608**, A72
 Ostriker E. C., Shu F. H., 1995, *ApJ*, **447**, 813
 Pfalzner S., Steinhausen M., Menten K., 2014, *ApJ*, **793**, L34
 Pollack J. B., Hubickyj O., Bodenheimer P., Lissauer J. J., Podolak M., Greenzweig Y., 1996, *Icarus*, **124**, 62
 Shapiro S. L., Teukolsky S. A., 1983, *Black holes, white dwarfs, and neutron stars : the physics of compact objects*. Wiley
 Spalding C., Batygin K., 2015, *ApJ*, **811**, 82
 Szulágyi J., Masset F., Lega E., Crida A., Morbidelli A., Guillot T., 2016, *MNRAS*, **460**, 2853
 Takata T., Stevenson D. J., 1996, *Icarus*, **123**, 404
 Tanigawa T., Ikoma M., 2007, *ApJ*, **667**, 557
 Tanigawa T., Tanaka H., 2016, *ApJ*, **823**, 48
 Tanigawa T., Ohtsuki K., Machida M. N., 2012, *ApJ*, **747**, 47

- Thanathibodee T., Calvet N., Bae J., Muzerolle J., Hernández R. F., 2019, arXiv e-prints, p. arXiv:1909.06450
 Turner N. J., Sano T., 2008, *ApJ*, **679**, L131
 Wagner K., et al., 2018, *ApJ*, **863**, L8
 Ward W. R., Canup R. M., 2010, *AJ*, **140**, 1168
 Yadav R. K., Thorngren D. P., 2017, *ApJ*, **849**, L12
 Zepolsky H. S., Salpeter E. E., 1969, *ApJ*, **158**, 809

APPENDIX A: DEGENERATE PLANETS

Electron degeneracy sets a floor on the radius $R_0 \approx R_J$ below which planets cannot contract (e.g. [Zapolsky & Salpeter 1969](#)). We therefore have to correct our scaling laws for the regime $R \lesssim 2R_0$, or equivalently $\Delta R/R_0 \lesssim 1$, where $\Delta R \equiv R - R_0$. This regime, in which degeneracy can no longer be neglected, is relevant for the late stages of contraction in the case of low opacities (see fig. 3 of [Ginzburg & Chiang 2019a](#)). The cooling time in this regime is given by

$$t_{\text{KH}} \sim \frac{GM^2}{R_0 L} \frac{\Delta R}{R_0}, \quad (\text{A1})$$

which replaces equation (2). In addition, degenerate planets need lose only a fraction $\sim \Delta R/R_0$ of their angular momentum to contract. Taking these two differences into account, equation (8) is replaced by

$$\frac{t_{\text{mag}}}{t_{\text{KH}}} \sim \left(\frac{P_{\text{break}}}{t_{\text{KH}}} \right)^{1/21} \left(\frac{\Delta R}{R_0} \right)^{19/21} < 1. \quad (\text{A2})$$

We conclude that for a given cooling time t_{KH} (in practice equal to the age of the system), degenerate planets spin down faster. However, using equations (A1), (1), and (4), their equilibrium rotation periods are closer to breakup:

$$\frac{P_{\text{max}}}{P_{\text{break}}} \sim \left(\frac{R_t}{R} \right)^{3/2} \sim \left(\frac{t_{\text{KH}}}{P_{\text{break}}} \right)^{1/7} \left(\frac{\Delta R}{R_0} \right)^{2/7}, \quad (\text{A3})$$

which replaces equation (9).

This paper has been typeset from a $\text{\TeX}/\text{\LaTeX}$ file prepared by the author.